Measurement of the neutrino mass using the inner bremsstrahlung emitted in the electron-capture decay of ^{163}Ho

P. T. Springer, C. L. Bennett, and P. A. Baisden
Lawrence Livermore National Laboratory, University of California, P.O. Box 808, Livermore, California 94550
(Received 14 July 1986)

An experimental investigation of the spectrum of x rays emitted in the electron-capture decay of ^{163}Ho is described. The data obtained are analyzed to determine their sensitivity to the value of the neutrino mass. At a 95% confidence level, an upper limit of 225 eV is set for the electron neutrino mass. No evidence for a finite value is found. Using available photon detectors, further improvements of this result are severely limited by uncertainties in atomic interference effects inherent to the decay.

I. INTRODUCTION

In modern physics, the implications of massive neutrinos are widespread. There is no established theoretical principle requiring neutrinos to be massless; in fact, certain grand unification theories naturally lead to massive neutrinos.[1,2] If neutrinos are massive, neutrinoless double-β-decay experiments can be used to determine if neutrinos are Dirac or Majorana particles.[3] Neutrino masses also allow the possibility of Cabibbo-like mixing among the neutrino types, and therefore neutrino oscillation[4] or decay. Although the most sensitive reactor experiments have failed to detect neutrino oscillations,[5] it could explain the discrepancy between the predicted and observed flux of high-energy (>0.8 MeV) neutrinos from the sun.[6,7] In cosmology, neutrino masses of even a few eV are important to the dynamics of the universe because of the abundance of primordial neutrinos. If the sum of the light (<3 MeV) neutrino types is greater than 3.5 eV, then the universe is neutrino dominated; if greater than 100 eV, then the universe is closed.[8] Galactic observations show that there is a considerable amount of nonluminous matter in the universe,[9,10] which cosmologists suggest may be a cloud of relic massive neutrinos.[11,12]

The most sensitive limits on the neutrino mass have come from tritium β-decay experiments. In these experiments, the spectral shape is examined near the end point for possible modifications of the phase-space factor due to a finite neutrino mass. In 1980, Lyubimov *et al.*[13] claimed to see evidence from their tritium measurements that the electron antineutrino has a nonzero rest mass of order 35 eV. Motivated by this claim, we began to investigate alternatives[14–16] potentially more sensitive to the neutrino mass. We report here our measurement of the electron-capture-decay properties of ^{163}Ho and its relevance to the mass of the neutrino.

II. USE OF ^{163}Ho IN A NEUTRINO MASS MEASUREMENT

Of all the isotopes which decay by electron capture, ^{163}Ho is perhaps the best suited for use in a neutrino mass measurement. ^{163}Ho decays by electron capture to ^{163}Dy with the lowest electron-capture Q value known. In ^{163}Ho, both K and L capture are energetically forbidden, therefore capture occurs through an M or higher shell. Because of the low Q value, the neutrino is emitted with low energy, and a neutrino mass of order 35 eV might have a pronounced effect on the decay properties.

In 1980, Bennett[14] first suggested that the relative capture rates of electrons in ^{163}Ho and in ^{161}Ho could be used as a neutrino mass probe, providing the Q value was favorable. However, following a precise measurement of the half-life,[17] a better estimate of the Q value was made that indicated that the relative capture ratio would have inadequate sensitivity to the neutrino mass. In addition, large interaction-energy shifts[18] have been observed in ^{163}Ho which prohibit the direct use of electron binding energies measured in photoemission experiments to interpret electron-capture data. The interaction-energy corrections to the Q value are of order 20 eV (see the Appendix). A similar interaction-energy correction to the neutrino mass would be of order 500 eV. Even small uncertainties in the interaction-energy shifts then produce major uncertainties in the neutrino mass. Thus, high-precision neutrino mass measurements would be very difficult to obtain from the relative capture ratio.

Another type of neutrino mass experiment, first discussed by De Rujula,[16] and the subject of this investigation, utilizes the spectral distribution of x rays emitted during electron-capture decays. During electron capture, x-ray radiation may occasionally accompany the emission of the neutrino in a process known as radiative capture or inner bremsstrahlung electron capture (IBEC). In radiative capture, an electron emits a photon during a virtual transition to an intermediate atomic state, and from that state, the electron is captured by the nucleus. The total transition amplitude is a coherent sum of the individual amplitudes from all possible intermediate states. The transition probability is then governed by a three-body phase-space factor similar to that of β decay. Analogous to the β-decay electron spectrum, the radiative-capture photon spectrum is continuous and extends to a maximum energy defined by the Q value for the reaction. Near the end point the shape of the photon spectrum, like

the electron spectrum, is sensitive to the mass of the neutrino.

For isotopes that decay by electron capture with moderate to high Q values, the radiative-capture spectral intensity near the end point is too low to be of practical use in a high-sensitivity neutrino mass experiment. However, the Q value for ^{163}Ho is in the x-ray region where the transition rates for radiative p capture are greatly enhanced. The enhancement is derived from the fact that the Q value is close in energy to a characteristic p to s x-ray transition. The closer the Q value is to the p to s x-ray energy, the greater is the sensitivity of the spectrum to the neutrino mass.

In the present investigation, the spectrum of x rays emitted from the radiative capture of $5p$ electrons in ^{163}Ho is measured with a solid-state, lithium-drifted silicon [Si(Li)] detector. The spectrum is then examined near its end point for the signature of a massive neutrino. Based on fits to the experimental spectrum, a neutrino mass limit of 225 eV is obtained at a 95% confidence level. The systematic errors in this upper limit are estimated to be of order 10 eV.

Uncertainties in the size of the atomic interference effects severely restrict a reduction of the neutrino mass limit derived from the x-ray spectrum of ^{163}Ho with the experimental method used. Significant increases in detector efficiency and resolution, however, might allow a more precise measurement of the atomic interference effects giving improved neutrino mass sensitivity.

III. THEORY OF RADIATIVE CAPTURE

In 1940, Morrison and Schiff calculated the continuous photon spectrum expected from radiative K capture. In 1956, Glauber and Martin[19] extended the theory to include the radiative capture of p electrons. Radiative p capture is much more intense in the x-ray region than is radiative s capture. Neglecting retardation and including the modifications appropriate for a massive neutrino, the spectral distribution expected from radiative p capture is given by

$$dw_{np}=q^2/(\pi^3 a)\mathrm{Tr}(N_{if}N_{fi})Q_{np}^{\,2}(k)k\,[k_{\max}(nl,v)+m_\nu-k]\{[(k_{\max}(nl,v)+m_\nu-k]^2-m_\nu^2\}^{1/2}dk\ , \tag{1}$$

where $Q_{np}(k)$ is given by

$$Q_{np}(k)=(\pi a/6)^{1/2}\sum_{n'}\frac{\psi_{n's}(0)(E_{n's}-E_{np})\langle n's\mid r\mid np\rangle}{(E_{n's}-E_{np}+k)}\ . \tag{2}$$

In these expressions, k is the photon energy, N_{fi} is the nuclear matrix element, a is the Bohr radius, m_ν is the neutrino mass; $k_{\max}(nl,v)$ is the radiative-capture end-point energy, $\psi_{ns}(0)$ is the amplitude of the ns orbital at the nucleus, E_{nl} is the energy of the nl level which is negative for the bound states and positive for the continuum states, $\langle n's\mid r\mid np\rangle$ is the radial matrix element of r, and the symbol $\sum_{n'}$ represents a sum over both the bound and continuum s states. The radiative-capture end-point energy is given by

$$k_{\max}(nl,v)=Q_{\mathrm{EC}}-E_{\mathrm{ex}}(nl,v)\ , \tag{3}$$

where Q_{EC} is the electron-capture Q value and $E_{\mathrm{ex}}(nl,v)$ is the excitation energy of the daughter atom with an nl hole and an extra valence electron v, given by Eq. (18) of the Appendix. In the previous and following expressions, we suppress all references to the spin-orbit splittings of the np levels.

A. Radiative capture in ^{163}Ho

The radiative-capture theory just described applies to direct transitions in which only a single photon accompanies the emission of the neutrino. In the decay of ^{163}Ho, the purely radiative transitions, which are important to the neutrino mass measurement, are the $5p$ to $3s$ and the $4p$ to $3s$. The spectral distributions of these x-ray transitions near their end points are sensitive to the neutrino mass. However, in general, the x-ray spectrum is complex since most of the other x rays are emitted along with electrons from Auger and Coster-Kronig transitions. The other x rays are found at lower energy than the purely radiative transitions of interest, and their spectral distributions are considerably more complex. Because of the energy shared with the electron(s), however, these x rays will not affect a neutrino mass measurement made near the end points of the purely radiative transitions, the $5p$ to $3s$ and $4p$ $3s$.

Equation (1) and a similar equation of Glauber and Martin for radiative s capture were used to calculate the spectrum from the radiative capture of $4p$, $5s$, $5p$, and $6s$ electrons in ^{163}Ho. The Hartree-Fock-Slater wave functions of Herman and Skillman were used to calculate the required dipole matrix elements and electron amplitudes at the origin. Empirical values were used for the energies and natural widths of the atomic states. For simplicity in the calculation of the radiative-p-capture spectra, we used only the term in Eq. (2) describing capture through the $3s$ level. The calculated spectra are shown in Fig. 1.

Above the approximately 2-keV $M_1O_{2,3}$ x-ray transition, the spectrum is dominated by the radiative capture of $5p$ electrons. Because of this, a coincidence experiment is not required, and we can compare the ^{163}Ho x-ray spectrum directly to the theoretical spectrum to determine the neutrino mass. Although radiative $5s$ and $6s$ captures have end-point energies comparable to the $5p$-capture end point, their intensities are typically less than 10^{-4} of the $5p$-capture intensity and thus can be ignored. The radiative $4p$ captures, however, cannot be ignored because their intensity is about 10% of the $5p$-capture intensity. Nevertheless, the $4p$-capture end-point energy lies well

below the $5p$ capture end point, and so the small corrections required can be easily applied. In the next section, we describe in detail the derivation of the inner bremsstrahlung spectrum for the radiative capture of $5p$ electrons in ^{163}Ho.

B. $5p$ radiative capture in ^{163}Ho

Incorporating the widths of the atomic levels, the transition amplitude for radiative $5p$ capture is found to be

$$Q_{5p}(k) \propto \sum_n \frac{(E_{ns}-E_{5p})\psi_{ns}(0)\langle ns \mid r \mid 5p\rangle}{(E_{ns}-E_{5p}+k+i\Gamma_{5pns}/2)} . \quad (4)$$

For photon energies k near the $5p$ to $3s$ transition energy, the summation for $Q_{5p}(k)$ is dominated by a single term describing capture through the $3s$ level. In that photon energy region, the radiative-capture spectral shape is just the Lorentzian line shape of the $5p$ to $3s$ transition. When the photon energy differs significantly from the $5p$ to $3s$ transition energy, levels other than the $3s$ contribute significantly to the $Q_{5p}(k)$ transition amplitude. We will refer to the coherent superposition of transition amplitudes from states other than the $3s$ as an "interference" to the transition amplitude from the $3s$ state. There are photon energies where the transition would be suppressed almost totally by the effects of this interference.

Separating the contribution of the $3s$ state to $Q_{5p}(k)$ from all other contributions gives

$$Q_{5p}(k) \propto \frac{(E_{3s}-E_{5p})}{(E_{3s}-E_{5p}+k+i\Gamma_{5p3s}/2)} + F(k) , \quad (5)$$

where

$$F(k) = \sum_{n\,(\neq 3)} \frac{(E_{ns}-E_{5p})\psi_{ns}(0)\langle ns \mid r \mid 5p\rangle}{(E_{ns}-E_{5p}+k)\psi_{3s}(0)\langle 3s \mid r \mid 5p\rangle} . \quad (6)$$

In the function $F(k)$, the widths of the intermediate states are neglected because they are so small relative to a typical energy spacing between the $5p$ and ns levels. The function $F(k)$ does not depend strongly on k near the $5p$ to $3s$ transition energy of $E_{5p}-E_{3s}$. For the purposes of this discussion, it is sufficient to treat $F(k)$ as constant and equal to

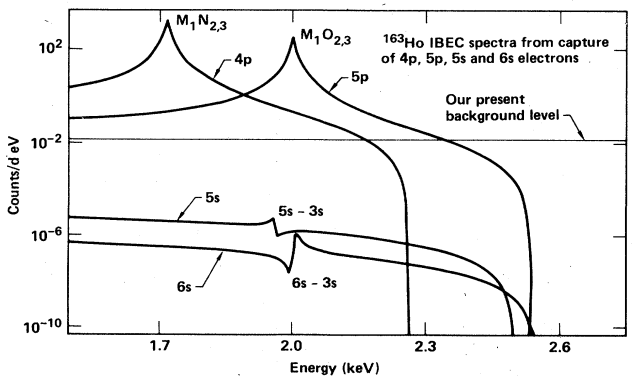

FIG. 1. Theoretical spectrum from radiative capture. Note the dominance of $5p$ capture above 2 keV.

$$F(k_{5p3s}) = \sum_{n\,(\neq 3)} \frac{(E_{ns}-E_{5p})\psi_{ns}(0)\langle ns \mid r \mid 5p\rangle}{(E_{ns}-E_{3s})\psi_{3s}(0)\langle 3s \mid r \mid 5p\rangle} . \quad (7)$$

In this approximation, the transition amplitude would have a "node" at a photon energy k_n given by

$$k_n = (E_{5p}-E_{3s})[1+1/F(k_{5p3s})] . \quad (8)$$

The real spectrum would not vanish at this photon energy since $F(k)$ and the amplitude from the $5p$ to $3s$ has imaginary components due to the finite lifetimes of the decaying states. Nevertheless, over a wide range of energies, the effect of interference can lead to large suppressions or enhancements of the radiative-capture transition rates.

C. Calculations of radiative $5p$ interference effects

Nonrelativistic calculations of the interference term $F(k_{5p3s})$ were performed using two different atomic models, the hydrogenic and the Hartree-Fock-Slater (HFS) models. We will first discuss the hydrogenic calculation.

For hydrogenic atoms, Gordon[20,21] derived a closed-form expression for $\langle nl \mid r \mid n'l-1\rangle$. Using this expression and the formula for $\psi_{ns}(0)$, the values of $\psi_{ns}(0)\langle ns \mid r \mid 5p\rangle$ were calculated for $n=1-1000$. Using the asymptotic limit of n^{-3} for the dependence of $\psi_{ns}(0)\langle ns \mid r \mid 5p\rangle$ on the principal quantum number n, the contributions of the remaining Rydberg states were obtained. For the continuum states which are described by a continuous parameter η, we used an analytical technique[22] to calculate $\psi_{\eta s}(0)\langle \eta s \mid r \mid 5p\rangle$. The absolute value of $\psi_{ns}(0)\langle ns \mid r \mid 5p\rangle$ was normalized by the number of s states per unit energy and plotted in Fig. 2(a) versus the energy of the intermediate s state. Note that the contribution from the $5s$ state is opposite in sign from all other contributions.

As a convenient check of the calculated values of $\psi_{ns}(0)\langle ns \mid r \mid 5p\rangle$ we used the sum rule

$$\begin{aligned}\sum_n \psi_{ns}(0)\langle ns \mid r \mid 5p\rangle &= \sum_n \int dr\, \psi_{ns}(0)\psi_{ns}(r) r\psi_{5p}(r) \\ &= \int dr\, \delta(r) r\psi_{5p}(r) \\ &= 0 . \end{aligned} \quad (9)$$

The sum rule was found to be satisfied at the level of one part in 10^8.

Given the values $\psi_{ns}(0)\langle ns \mid r \mid 5p\rangle$ for all the bound and continuum states, the evaluation of $F(k)$ was performed. Table I illustrates the contributions to the interference term $F(k_{5p3s})$ of the various hydrogenic intermediate states. Using the hydrogenlike approximation, and assuming that $F(k)$ is independent of x-ray energy near the $5p$ to $3s$ transition, the theoretical ^{163}Ho $5p$ radiative-capture transition rate was found to be suppressed by more than a factor of 2 in the end point region. The higher Rydberg and the continuum states contribute significantly to the interference.

A similar calculation was performed using the nonrelativistic Hartree-Fock-Slater model of Herman and Skillman for dysprosium. This calculation was performed in

TABLE I. Contributions to $F(k_{5p3s})$ in hydrogenic and HFS atomic models.

ns level	$\frac{(E_{ns}-E_{5p})\psi_{ns}(0)\langle ns \mid r \mid 5p\rangle}{(E_{ns}-E_{3s})\psi_{3s}(0)\langle 3s \mid r \mid 5p\rangle}$ Hydrogenic	HFS
$1s$	0.518 334	0.3429
$2s$	0.951 427	0.6974
$4s$	−1.133 289	−0.4443
$5s$	0.000 000	0.1333
$6s$	0.170 018	0.0184
$7s+\cdots$	0.233 172	0.0068
Continuum	0.570 599	1.01±0.03[a]
Total	1.310 261	1.76

[a]Numerical accuracy.

order to investigate the effect of screening on the interference term. Dysprosium wave functions were used because, neglecting the interaction energy shifts, the x rays emitted from ^{163}Ho are characteristic of dysprosium. The radial wave functions were calculated using the Noumerov method[23] to numerically integrate the Schrödinger equation in the screened potential. As a test, the screened potential was replaced by the hydrogenic potential, and the values of $\psi_{\eta s}(0)\langle \eta s \mid r \mid 5p\rangle$ reproduced the hydrogenic values to the level of 0.1%. Higher levels of accuracy could be achieved with a smaller integration step size.

With the Herman and Skillman tabulated radial wave functions for the bound states, the values of $\psi_{ns}(0)\langle ns \mid r \mid 5p\rangle$ were calculated for $n=1$—6. Using the calculated continuum radial wave functions, and the tabulated $5p$ radial wave function, the values of $\psi_{\eta s}(0)\langle \eta s \mid r \mid 5p\rangle$ were calculated for continuum energies between 10^{-4} eV and 50 keV. The asymptotic limit for the dependence of $\psi_{\eta s}(0)\langle \eta s \mid r \mid 5p\rangle$ on η was used to determine the contributions from continuum states above 50 keV and below 10^{-4} eV. The sum rule [Eq. (9)] was used to determine the contributions of all higher Rydberg states. Figure 2(b) shows the absolute value of $\psi_{ns}(0)\langle ns \mid r \mid 5p\rangle$, normalized by the number of s states per unit energy, and plotted versus the energy of the ns state. This figure is analogous to Fig. 2(a) except it pertains to dysprosium rather than hydrogen. Again, the $5s$ contribution is opposite in sign from all others.

With the values of $\psi_{ns}(0)\langle ns \mid r \mid 5p\rangle$ calculated for dysprosium, and assuming that the unoccupied high Rydberg states all lie at zero energy, $F(k)$ was evaluated. In Table I, the contributions to the interference term in the HFS model are compared to the contributions in the hydrogenic model.

Figure 3 shows the square of the transition amplitude for the radiative capture of the holmium $5p$ electrons near the $M_1O_{2,3}$ resonance, with and without the effect of interference included. In calculating the interference effects shown in the figure, only the $1s$ to $6s$ levels were considered. Near the $5p$ radiative-capture end point, the transition rates were found to be suppressed by about a factor of 2 due to interference from the bound states. When the

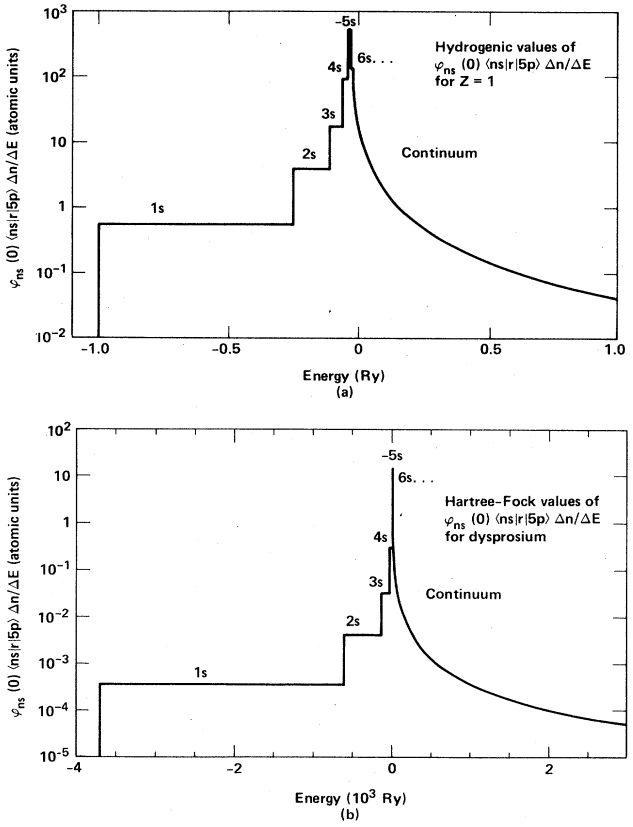

FIG. 2. Calculated values of $\psi_{ns}(0)\langle ns \mid r \mid 5p\rangle$ using (a) hydrogenic and (b) Hartree-Fock-Slater atomic models.

contributions to the interference from the high Rydberg and the continuum states are also included, the suppression increases to almost a factor of 4.

Riisager[24] has performed a similar calculation using a sum-rule method. This method accounts for the high Rydberg and continuum states in an approximate manner.

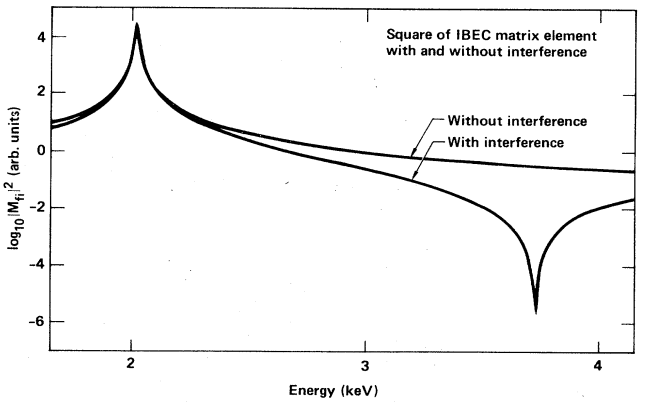

FIG. 3. The IBEC matrix element squared showing the effects of the interference suppressions from the $1s$ through $6s$ states. Interference from the high Rydberg and continuum states further suppress the spectrum, moving the interference node from 3.7 to 3.1 keV.

The resulting interference term is about 25% higher than in the treatment described above.

IV. EXPERIMENT

A 30-mm^2 lithium-drifted silicon detector was used to measure the x-ray spectrum since it provided an acceptable compromise between geometrical efficiency (about 4%) and energy resolution [about 137 eV full width at half maximum (FWHM) at 2 keV]. The detector was shielded in a lead cave lined with both cadmium and copper. In addition to acoustically isolating the Si(Li), data collection was inhibited when excessive audio noise was detected. This significantly reduced the background count rate at low energies. The background spectrum was carefully measured to allow precise subtraction from the observed x-ray spectrum. No characteristic x-ray lines which might interfere with our measurements were detected in the background spectrum.

Both the energy response and the resolution of the Si(Li) detector were measured by exciting K x rays in targets of aluminum, silicon, phosphorus, sulfur, chlorine, calcium, and titanium using a 10-mCi ^{55}Fe x-ray fluorescence source. These targets were chosen to completely cover the x-ray region of interest for the ^{163}Ho decay. In addition, calibrated sources of ^{55}Fe and ^{49}V provided low-background K x-ray spectra for magnesium and titanium. The observed $K\alpha$ and $K\beta$ lines were fit with Gaussian peaks and the observed centroids and widths were corrected for the splittings between the unresolved $K\alpha_1$ and $K\alpha_2$ lines. The calibration was found to be linear with a mean squared deviation of about 2.25 eV^2.

We typically accumulated data using the ^{163}Ho source for periods of about two weeks. Calibrations were performed before and after each accumulation of data. The calibration was found to be stable against gain drifts at the level of about 0.25 eV/week.

The detector variance, the square of the Gaussian width parameter σ, was found to vary approximately linearly with energy, as is shown in Fig. 4. However, a discontinuity in the detector variance was observed between the energies of the silicon and phosphorus K x rays (the aluminum and silicon points are not included in the fit). We presume that the observed discontinuity occurs because of the difference in x-ray penetration depth and photoelectron energy for x rays above and below the silicon K-electron binding energy of 1840 eV. No such discontinuity was found in the energy calibration.

The ^{163}Ho source material was produced by neutron activation of an enriched ^{162}Er target at the high-flux beam reactor (HFBR) of Brookhaven National Laboratory. Following two chemical separations,[17] the ^{163}Ho was isotope separated to reduce the ^{166m}Ho contamination in the sample to an acceptable level. The radioactive contaminant ^{166m}Ho had been produced by neutron activation of trace amounts of natural holmium in the erbium target. The holmium was dissolved, precipitated in the form of $^{163}HoF_3$, and then vacuum-evaporated onto a stainless-steel substrate to produce the ^{163}Ho source used in our measurement.

The total amount of holmium on the source was measured by x-ray fluorescence. A ^{109}Cd source was used to excite the holmium $K\alpha_1$ and $K\alpha_2$ x rays, which were then detected and recorded. A known quantity of natural holmium was fluoresced in a similar manner, and a comparison of the $K\alpha$ fluoresence rates gave a value of 89.7±9 μg for the total amount of ^{163}Ho on the source.

A crude measure of the $^{163}HoF_3$ source distribution was inferred from the positions of colored bands visible in the source. The color of light reflecting from the $^{163}HoF_3$ source depends upon the source thickness due to the optical interference of light which reflects from the top and bottom surfaces. Dana[25] reported the color versus thickness for quartz, and this was used to give the relative thickness versus position in the $^{163}HoF_3$ source. The source thickness was then normalized to the total amount of ^{163}Ho determined by the x-ray fluorescence measurement.

The experimental setup is shown schematically in Fig. 5. In order to reach the detector, the x rays must pass through various materials: the source material (30 μg/cm^2), a layer of air (250 μg/cm^2), a beryllium en-

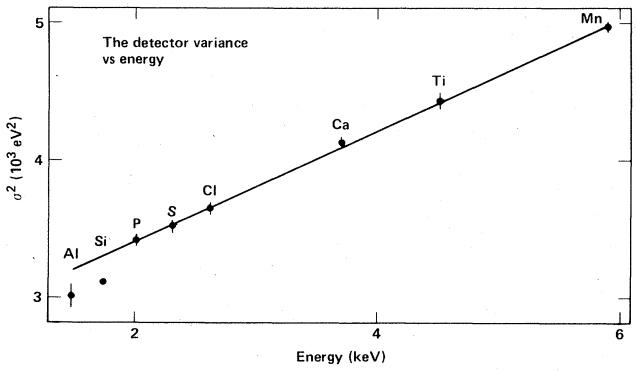

FIG. 4. The Si(Li) detector variance σ^2 as a function of energy. Note the anomalous behavior of σ^2 for x rays below the 1.84-keV silicon K binding energy.

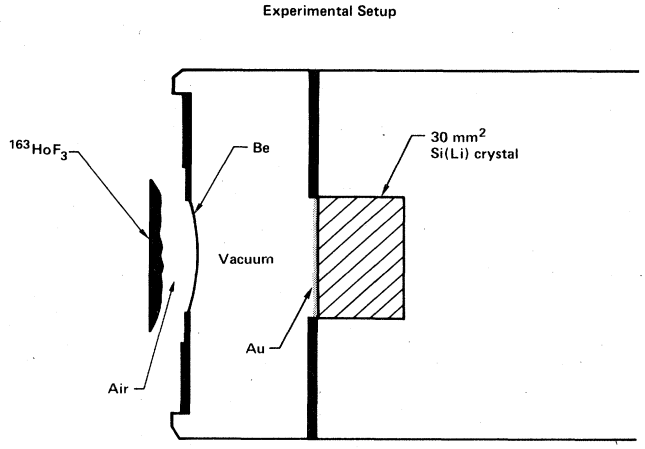

FIG. 5. The experimental setup showing the placement of the source with respect to the Si(Li) detector.

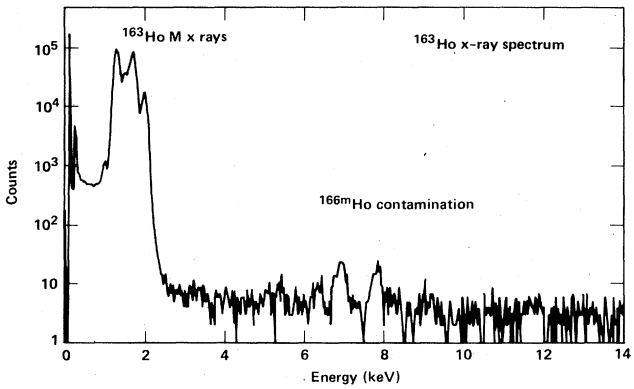

FIG. 6. The ^{163}Ho x-ray spectrum with erbium L x rays from a slight ^{166m}Ho contamination. The ^{166m}Ho x-ray spectrum is flat in the 2—3 keV region of interest for the neutrino mass measurement.

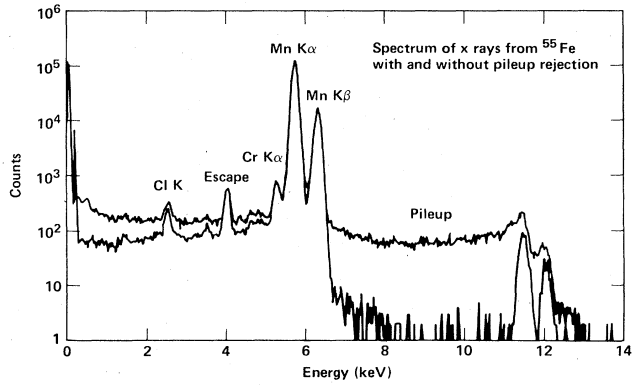

FIG. 8. The spectrum of ^{55}Fe illustrating the detector response which is characterized by photopeaks, incomplete charge collection tails, escape peaks, and pileup.

trance window (1.4 mg/cm^2), an evacuated region, and a gold contact layer on the Si(Li) crystal (40 μg/cm^2). An additional layer of beryllium (4.37 mg/cm^2) was placed between the source and detector to eliminate potential pileup problems.

Figure 6 shows the ^{163}Ho x-ray spectrum measured over a 23.53-day period with the use of pileup rejection. In addition to ^{163}Ho x rays, the spectrum shows erbium L x rays from the small residual ^{166m}Ho contamination in the source. The x-ray spectrum of ^{166m}Ho was measured independently to investigate potential background problems. No lines of significant intensity between 2 and 3 keV were observed for the ^{166m}Ho spectrum. We observed only a flat background which contributed about 20% of the background counts between 2.5 and 3 keV.

Figure 7 shows the ^{163}Ho x-ray spectrum in the region from about 1 to 2 keV. In this figure, the dots represent the observed number of counts per channel, and the solid curve represents the result of fitting the data with a series of Gaussian peaks whose positions and magnitudes are represented by the vertical lines drawn under the spectrum. Although the spectrum is comprised of many different transitions, only five major groups of transitions are observed because the x-ray splittings are small relative to the resolution of the Si(Li). The lowest energy group, the $M\zeta$ at about 1 keV, is missing from the figure.

The observed ^{163}Ho x-ray spectrum is the result of modifications of the theoretical spectrum by the response of the detector, and it is therefore important to understand these modifications. The response is characterized by photopeaks, incomplete charge collection tails, escape peaks, and pileup, as illustrated in Fig. 8. For clarity, we have shown the spectrum taken both with and without pileup rejection.

The photopeak shape was measured with the spectrum of silicon $K\alpha$ and $K\beta$ x rays. The data is shown in Fig. 9 along with a fit using a Gaussian response. There were no significant deviations from Gaussian behavior down to the level of the statistical fluctuations in the background counting rate. Independent measurements of the expected backgrounds showed that the photopeak shape was Gaussian on the high-energy side to at least the level of 10^{-4} from the peak height. Above the $M_1O_{2,3}$ line in ^{163}Ho, the inner bremsstrahlung is resolved from the

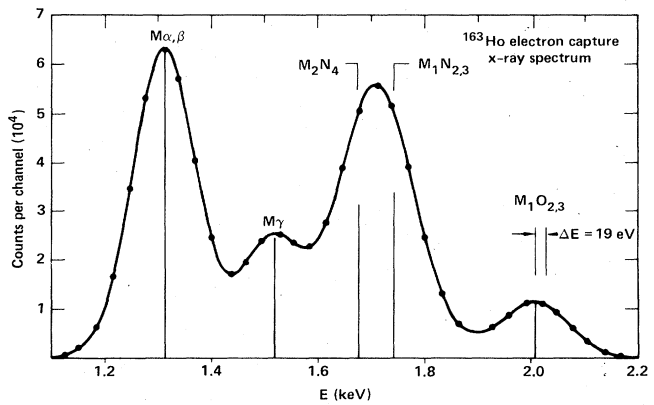

FIG. 7. The ^{163}Ho x-ray spectrum in the 1—2 keV region and a fit using Gaussian peaks. The $M\zeta$ peak at approximately 1 keV is not shown in the figure.

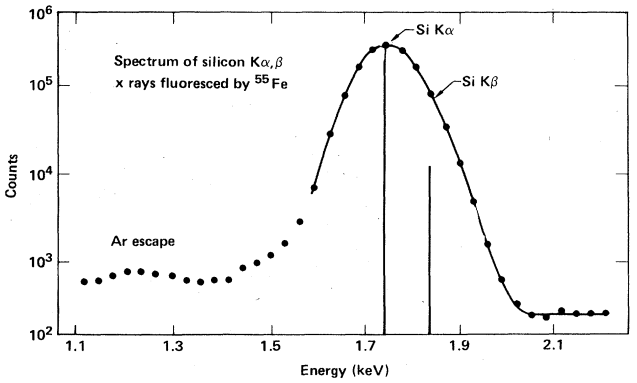

FIG. 9. The spectrum of silicon K x rays and a fit using Gaussian peak shapes. On the high-energy side of the x-ray peak, the response was found to be Gaussian down to 10^{-4} from the peak height.

Gaussian tails of the $M_1O_{2,3}$ peak at about the 10^{-2} level from the peak height, and so a Gaussian description of the photopeak shape on its high-energy side should be adequate.

The effects of the incomplete charge collection tail and the silicon escape losses on the neutrino mass measurement were estimated using the K x-ray spectra of silicon, sulfur, chlorine, argon, titanium, and manganese. The total intensity in the incomplete charge collection tail was between 1.5% and 4.5%. If ignored, the spectral modifications introduced by the tailing would limit the neutrino mass sensitivity to about 20 eV. The energy dependence of the total photopeak intensity loss was found to be less than 2%/keV in the ^{163}Ho end-point region. If this energy-dependent efficiency loss were ignored, the neutrino mass sensitivity would be limited to approximately 50 eV.

The silicon escape losses were modeled in a manner similar to Russ[26] and found to agree well with the measured losses. In the ^{163}Ho end-point region the silicon escape losses were about 1.5%. The "escape spectrum" lies at too low an energy to affect the neutrino mass measurement. The energy dependence of the silicon escape loss was found to be 0.4%/keV in the ^{163}Ho end-point region. If this energy-dependent efficiency loss were ignored, the neutrino mass sensitivity would be limited to approximately 23 eV.

A computer program was used to simulate the expected pileup, using the Si(Li) pulse shape measured with sulfur K x rays. The predicted pileup spectrum was found to agree with the pileup shown in Fig. 8 at the 10% level. For the 3 counts/sec counting rate of the ^{163}Ho source, the predicted pileup in the end-point region was at the level of the background counting rate. With the use of pileup rejection and a 4.37 mg/cm^2 beryllium attenuator to reduce the rate of lower-energy x rays, the pileup was virtually eliminated.

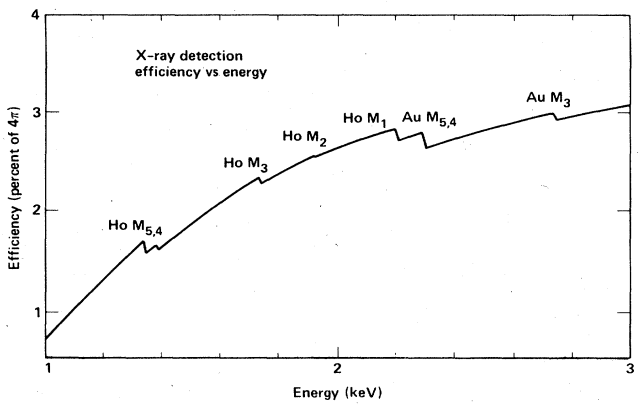

FIG. 10. The calculated x-ray detection efficiency used to account for x-ray absorption. In this example the geometrical efficiency is approximately 3.7%.

X-ray absorption also modifies the theoretical spectrum. In order to apply corrections for this, the efficiency for detecting a photon emitted randomly throughout the $^{163}HoF_3$ source was calculated numerically as a function of energy. This calculation required the use of the thicknesses and distributions of the materials between the source and the detector. Figure 10 shows the calculated x-ray detection efficiency without the 4.37 mg/cm^2 beryllium attenuator.

V. DATA ANALYSIS

A. Creating a model spectrum

The theoretical inner bremsstrahlung spectrum $S_{\text{theor}}(k)$ from the radiative capture of $4p$ and $5p$ electrons is given by the following:

$$S_{\text{theor}}(k)=A_{4p}Q_{4p}^2(k)k[k_{\max}(4p,4f)+m_\nu-k]\{[k_{\max}(4p,4f)+m_\nu-k]^2-m_\nu^2\}^{1/2}$$
$$+A_{5p}Q_{5p}^2(k)k[k_{\max}(5p,4f)+m_\nu-k]\{[k_{\max}(5p,4f)+m_\nu-k]^2-m_\nu^2\}^{1/2}\,, \tag{10}$$

where A_{4p} and A_{5p} are normalizing constants, and $k_{\max}(nl,4f)$ is the end-point energy. The expression used for $Q_{5p}(k)$ is

$$Q_{5p}(k)=\frac{-k_{5p\,3s}}{(k-k_{5p\,3s}+i\Gamma_{5p\,3s}/2)}+F(k)\,, \tag{11}$$

where $F(k)$ represents an interference term which does not depend strongly on energy near the $M_1O_{2,3}$ transition energy $k_{5p\,3s}$. For the purposes of fitting the data, $F(k)$ was approximated by a constant equal to the value of $F(k)$ at the peak energy $k_{5p\,3s}$. A similar expression for $Q_{4p}(k)$ is

$$Q_{4p}(k)=\frac{-k_{4p\,3s}}{(k-k_{4p\,3s}+i\Gamma_{4p\,3s}/2)}\,. \tag{12}$$

To account for the effects of interference in radiative $4p$ capture, the expression for $Q_{4p}(k)$ should also include a function analogous to $F(k)$. The interference effects in $4p$ capture are expected to be smaller than in $5p$ capture since the dipole matrix element $\langle 4p \mid r \mid 3s \rangle$ is larger. For this reason and because the corrections would be small, we have neglected the effects of the interference in $4p$ capture.

In order to compare a theoretical spectrum to data, the theoretical spectrum must be modified to account for the effects of efficiency, resolution, and analog to digital converter (ADC) binning. To do this, we first multiply the theoretical spectrum of Eq. (10) by the energy-dependent detection efficiency. Next, we perform a convolution of the resulting spectrum and the Gaussian detector response

function. Finally, we integrate this smoothed spectrum into bins corresponding to the channels of the ADC. As a test, the convolution routine was used to perform the convolution of a Lorentzian and a Gaussian, and the result was found to agree with the analytical solution, the real part of the complex error function, described by Abramowitz and Stegun.[27]

B. Fitting the data

The raw data are the x-ray spectrum shown in Fig. 6. The only portion of this spectrum sensitive to the neutrino mass is the energy region near 2 keV, and the fitting region extended from 1.94 to 3.29 keV. Before the spectrum in this region can be examined for the effects of a neutrino mass, the slight influence of the lower-energy peaks must be removed. In order to do this, the entire spectrum was fit to a series of Gaussian peaks, as shown in Fig. 7, and the peaks labeled $M\alpha, \beta$, $M\gamma$, and M_2N_4 were subtracted from the data. The resulting spectrum contained only the $4p$ to $3s$ and $5p$ to $3s$ peaks, and was used in fits to determine the neutrino mass. In the fitting region, from 1.94 to 3.29 keV, the spectrum was not significantly affected by the subtraction of the lower energy peaks.

When fitting the observed spectrum with a calculated one, the following quantities were not allowed to vary because they were well determined by other measurements; the x-ray detection efficiency versus energy, the calibration, the detector resolution versus energy, the background spectrum, and the energy and relative intensity of the $M_1N_{2,3}$ line. The model parameters allowed to vary in a fit include the following: the number of counts N in the $M_1O_{2,3}$ line, the value of the ^{163}Ho-^{163}Dy mass difference δM which equals $Q_{\rm EC}+m_\nu$, the square of the neutrino mass m_ν^2, the interference term $F(k_{5p3s})$, the $M_1O_{2,3}$ linewidth Γ_{5p3s}, and the $M_1O_{2,3}$ transition energy k_{5p3s}.

The fits were found to be relatively insensitive to the value of the $M_1N_{2,3}$ linewidth. In the fits discussed below, the value for the $M_1N_{2,3}$ linewidth was set to 15 eV.

With $Q_{\rm EC}$, m_ν and $F(k_{5p3s})$ as free parameters in a fit, little sensitivity to the neutrino mass was observed since the parameters were strongly correlated. However, $Q_{\rm EC}$ can be constrained on the basis of independent measurements. Hartmann[28] measured the relative capture rates of N and M electrons in ^{163}Ho using a high-temperature proportional counter and determined the value of $Q_{\rm EC}$. We have reanalyzed Hartmann's data to account for the dynamic interaction energy shifts in the characteristic x-ray spectrum, and obtain $Q_{\rm EC}=2561\pm20$ eV (statistical error only) for $m_\nu=0$ (see the Appendix). Although the value of $Q_{\rm EC}$ deduced from the M to N ratio depends linearly on the neutrino mass assumed, the value of $\delta M=Q_{\rm EC}+m_\nu$ has only a second-order dependence on neutrino mass. For $m_\nu<250$ eV, the 2σ (s.d.) upper limit of δM is less than 2640 eV.

Ravn *et al.*[29] also measured the total absorption spectrum by implanting ^{163}Ho in a Si(Li) detector. They deduced a Q value of $2.82^{+0.11}_{-0.08}$ keV, which is in poor agreement with Hartmann's value. This lack of agreement can perhaps be attributed to poor charge collection. In Ravn's experiment, the detector failed in a few days time. In the data collected, the peak from M capture events was 200 eV below its expected position, so the M electrons lost about 200 eV in traveling to an active region of the Si(Li) crystal. Following N capture, the total energy of the ejected electrons is only about 400 eV, and these electrons will also lose energy. The straggling on the N peak would have been difficult to observe because of the amplifier noise, and so the N peak intensity may have been underestimated. For these reasons, we believe that Hartmann's data are more reliable, and therefore we have used them in our analysis.

In the five fits shown in Table II, the values of the $M_1O_{2,3}$ line intensity N, width Γ_{5p3s}, and energy k_{5p3s} were allowed to vary. The best-fit values for N, Γ_{5p3s}, and k_{5p3s} did not vary significantly from fit to fit. The $M_1O_{2,3}$ line contains about 118 000 counts, has a width of $10.5\pm1,\pm1$ eV, and has an energy of $2005.0\pm0.5,\pm1.5$ eV, where the errors quoted are statistical and systematic, respectively.

All of the fits achieved an acceptable value of χ^2. In fit 1, for 41 degrees of freedom, the χ^2 per degree of freedom was 0.82. When the fit was performed with the errors being (theory)$^{1/2}$ rather than (data)$^{1/2}$, the total χ^2 per degree of freedom increased to 0.97, but the fit parameters were not significantly affected.

Figure 11 shows the data for fit 1 of Table II and represents a typical fit. Although the region of interest was from 1.94 to 3.29 keV, the fitted curve was extended to lower energies to verify that it represents the data fairly well even in the $M_1N_{2,3}$ peak. Figure 12 shows the same data and fit transformed into a plot analogous to the Kurie plot for β decay. To obtain the plotted curve the following expression was used:

$$N_{\rm Kurie}(k)=[N(k)/N_Q(k)]^{1/2}\ . \tag{13}$$

TABLE II. Fit parameters in IBEC analysis.

Fit no.	δM Value (eV)	δM Error (eV)	m_ν Value (eV)	m_ν Error (eV)	$F(k_{5p3s})$ Value	$F(k_{5p3s})$ Error	χ^2	Degrees of freedom
1	2623	40	0	fixed	0.00	fixed	33.66	41
2	2728	35	0	fixed	1.76	fixed	32.54	41
3	2713	140	0	fixed	1.5	2.6	32.51	40
4	2565	fixed	0	fixed	−0.59	0.7	34.72	41
5	2640	fixed	0	100	0.51	0.6	33.17	40

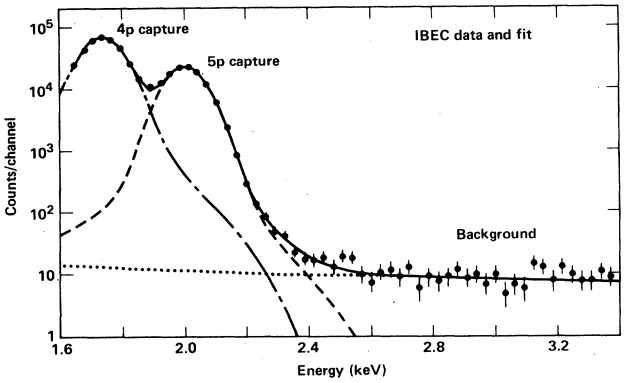

FIG. 11. ^{163}Ho x-ray data and a typical fit (fit 1). The solid curve represents a model spectrum which has corrections for absorption, detector resolution, and ADC binning. Also shown are the separate contributions from $4p$ capture, $5p$ capture, and measured backgrounds.

Here $N_Q(k)$ is the spectrum obtained from Eq. (10) when the $(k_{\max}-k)^2$ phase-space variation is ignored. For simplicity, $N_Q(k)$ was approximated by the following analytical expression:

$$N_Q(k)=N(2\pi\sigma^2)^{-1/2}[\mathrm{Re}w(z)+\Gamma_{5p\,3s}(2k_{5p\,3s})^{-1}\mathrm{Im}w(z)] \, . \tag{14}$$

Here N is the number of counts in the $5p$-$3s$ line; σ is the Gaussian detector width; and $w(z)$ is the complex error function[27] with

$$z=(k-k_{5p\,3s})(2\sigma^2)^{-1/2}+i\Gamma_{5p\,3s}(8\sigma^2)^{-1/2} \, . \tag{15}$$

In the region that is resolved from the Gaussian peak of the $M_1O_{2,3}$ both the data and the fit resemble a line that approaches a value of zero near 2.6 keV. The nonlinear behavior near the end point is due to the detector resolution. Also drawn is the expected spectrum if the neutrino mass were 300 eV and all other parameters were unchanged.

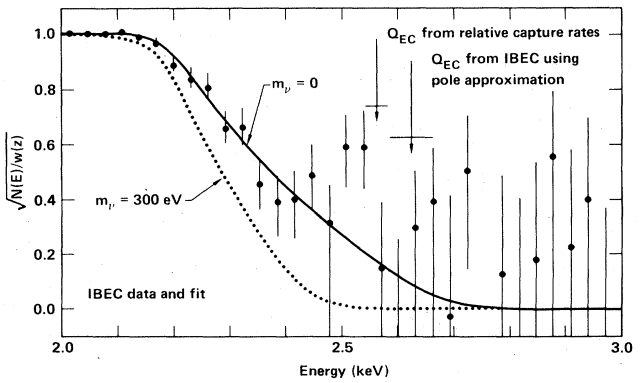

FIG. 12. Data and fit of Fig. 11, but transformed to a plot analogous to the Kurie plot of beta decay. The Q values indicated by this fit and by the relative capture ratio data are shown on the plot. Also drawn is the spectrum expected if the neutrino mass were 300 eV.

Fits 1–3 are used to investigate the sensitivity of Q_{EC} to the interference term $F(k_{5p\,3s})$, for a massless neutrino. We investigated three cases: when the interference term was set to zero, when it was set to the HFS prediction of 1.76, and when it was unconstrained. The resulting Q values were, respectively, 2623 ± 40 eV, 2728 ± 35 eV, and 2713^{+190}_{-95} eV (with 2σ limits of 2713^{+215}_{-202} eV). The value of the interference term was found to be strongly correlated with the value of Q_{EC}. The statistical uncertainty in Q_{EC} for a particular choice of the interference term is much smaller than the range of Q_{EC} allowed with no constraints on the interference term. Also, the range of possible values for Q_{EC} overlaps with the value of 2561 ± 20 eV determined using the N to M capture ratio data of Hartmann.

With Q_{EC} constrained to be within the range allowed by the M to N capture ratio data, the range of values for the interference term is not consistent with the atomic physics prediction of 1.76, as can be seen in fit 4 of Table II. We regard the analysis of the M to N capture rate data as more reliable than the atomic physics theoretical calculation, and are thus forced to let the interference amplitude remain a free parameter.

In fit 5, we allow the neutrino mass to vary, but constrain δM ($\delta M=Q_{\mathrm{EC}}+m_\nu$) to 2640 eV, the upper limit allowed by Hartmann's data for a neutrino mass as large as 250 eV. The interference term was also allowed to vary. Requiring m_ν^2 to be greater than zero, the minimum value of χ^2 occurs at a value for m_ν of zero. The 1σ and 2σ limits for the neutrino mass are 100 and 225 eV, respectively. The 2σ upper limit is one-sided and corresponds to a confidence interval of 95%. The value of χ^2 for the fit is 33.17 which is only 0.66 greater than that of fit 3 in which both the Q value and the interference term were varied with the neutrino mass set to zero. We do not believe that this difference in χ^2 is significant, and so conclude that δM had not been constrained at too low a value.

We observed that the upper limit for the neutrino mass was very insensitive to changes in the model parameters that were constrained during the fit. For example, by using the upper limit on the detector variance, the $M_1O_{2,3}$ linewidth parameter $\Gamma_{5p\,3s}$ decreased from 10.6 to 9.5 eV, and the upper limit on the neutrino mass increased by only 6 eV. When the parameter for the $M_1N_{2,3}$ linewidth $\Gamma_{4p\,3s}$ was changed from 15 to 10 eV, the $M_1O_{2,3}$ linewidth parameter $\Gamma_{5p\,3s}$ increased from 10.6 to 11.5 eV, and the upper limit on the neutrino mass decreased by only 6 eV. Using the uncertainty in the background counting rate of 1 count per channel, negligible corrections to the upper limit for the neutrino mass were found. The uncertainties in the thicknesses of the beryllium window and the gold contact layer also had a very small affect on the calculated upper limit for the neutrino mass. To illustrate this, a fit was performed in which the absorption in the 4.37 mg/cm^2 beryllium foil was neglected entirely. The thickness of this beryllium foil was over three times the nominal thickness of the beryllium entrance window. With this important attenuation correc-

tion neglected, the upper limit on the neutrino mass decreased by only 1 eV. This result is dependent on constraining the value of δM. A nominal error of 30% in the thickness of the beryllium entrance window and gold contact layer would limit the sensitivity to the neutrino mass to about 75 eV.

If the parameter for the neutrino mass squared were not constrained to be positive, then the upper limit for the neutrino mass would depend more strongly upon the assumptions of the model, but in all cases would still be less than 225 eV. Also, the limit would improve if a smaller value were assumed for δM. Choosing the upper limit from Hartmann's measurement yields the most conservative limit for the neutrino mass.

The 225-eV upper limit for m_ν depends on the 2640-eV constraint for δM. If further experimentation were to show that δM is larger than Hartmann's measurement indicates, then our analysis would require modification. If the N/M ratio were that found by Ravn *et al.* then the 2σ upper limit of δM would increase to about 2913 eV, and the 2σ upper limit for the neutrino mass would increase to about 500 eV.

VI. CONCLUSIONS

In this investigation, the spectrum of x rays emitted during the electron-capture decay of ^{163}Ho was measured with a solid state Si(Li) detector. The shape of this spectrum near the end point was used to infer an upper limit for the neutrino mass. For the detector the response function, the energy calibration, and the resolution were carefully investigated. Above the highest energy line ($M_1O_{2,3}$), the spectrum is dominated by the radiative capture of $5p$ electrons. A theoretical $5p$ radiative capture spectrum with experimental corrections was calculated and compared with the observed spectrum. If the electron-capture Q value determined in an independent measurement by Hartmann is used, the interference suppressions are found to be smaller than the Hartree-Fock-Slater predictions. We believe that this discrepancy indicates that the atomic models used in the calculations are inadequate. Using the observed ^{163}Ho x-ray spectrum and an unconstrained interference term, a neutrino mass limit of 225 eV is obtained, at a 95% confidence level. No evidence for a finite value is found. The systematic errors in this upper limit are of order 10 eV.

A significant improvement in the neutrino mass limit would require both an improvement in detector resolution and in the counting rate. The major limitation in the present measurement, in addition to the statistical uncertainty, is the uncertainties in the size and direction of the interference effects. As the calculations of the interference effects are unreliable, $F(k)$ must be determined in a simultaneous fit with m_ν and Q_{EC}. The poor resolution of the present detector prohibits this. It might be possible to decouple the effects of interference from the measurement of the neutrino mass if detectors were available having greatly improved efficiency and resolution. In consideration of available technology, tritium β-decay experiments remain the most sensitive measure of the electron (anti-)neutrino mass.

APPENDIX: DETERMINATION OF Q_{EC} FROM THE N to M CAPTURE RATIO OF ^{163}Ho

Recently, Hartmann[28] independently determined the Q value for electron capture, Q_{EC}, for ^{163}Ho from the ratio of the capture rates of the M and N electrons. Hartmann reported

$$\lambda_N/\lambda_M = 3.86 \pm 0.12 ,$$

where λ_N is the total capture rate of N electrons and λ_M is the total capture rate of M electrons. Using atomic binding energies derived from photoemission experiments, Hartmann deduced a value for Q_{EC} of 2600 ± 30 eV. However, the excitation energies of the atomic states reached by electron capture are shifted with respect to those of the states reached by photoemission.[18,30] The shifts are caused by the presence of an additional valence electron left by the parent atom in the case of electron capture. These shifts must be included in an accurate analysis of electron-capture data.

The theoretical capture ratio of electrons from orbitals i and j is given by

$$\lambda_i/\lambda_j = (q_i p_i W_i \beta_i^2 B_i)/(q_j p_j W_j \beta_j^2 B_j) , \tag{A1}$$

where q_i is the occupancy, p_i and W_i are the momentum and total energy of the emerging neutrino, β_i is the Coulomb amplitude of the electronic bound state, and B_i is the overlap and exchange correction. The relation between the neutrino momentum and total energy is given by

$$p_i^2 = [\delta M - E_{\mathrm{ex}}(i,v)]^2 - m_\nu^2 = W_i^2 - m_\nu^2 . \tag{A2}$$

In this expression, δM is the difference in mass between the neutral parent atom and the neutral daughter atom which equals $Q_{\mathrm{EC}} + m_\nu$, m_ν is the neutrino mass, and $E_{\mathrm{ex}}(i,v)$ is the excitation energy of the atomic state reached by the capture of electron i.

In the frozen-orbital approximation, the configuration-average excitation energy is given by

$$E_{\mathrm{ex}}(i,v) = -E_i + E_v + V(v,v) - V(i,v) , \tag{A3}$$

where E_i is the single-particle energy of electron i for the daughter atom in its ground-state configuration, v symbolizes the valence electron shell, and $V(i,j)$ is the interaction energy between electrons i and j, defined by Slater.[30]

Table III shows the atomic parameters used in our analysis. The values of E_i were obtained from the x-ray

TABLE III. Atomic parameters for N to M capture ratio analysis.

Shell	$-E_i$ (eV)	$E_{\mathrm{ex}}(i,4f)$ (eV)	β_i (atomic)	B_i
M_1	2046.8	2029.3	0.222 52	1.065
M_2	1841.8	1824.2	0.051 04	0.935
N_1	416.3	406.7	0.107 41	1.12
N_2	331.8	322.6	0.024 27	0.88

tables of Bearden.[31] $E_{4f}=-5.2$ eV was obtained from the relaxed-orbital calculations of Huang *et al.*[32] The interaction energies $V(i,j)$ were evaluated using the Herman and Skillman[33] Hartree-Fock-Slater wave functions for dysprosium. The values of the Coulomb amplitudes and the overlap and exchange correction factors were obtained from Bambynek.[34]

Assuming $m_\nu=0$, a value of 2561 ± 20 eV is deduced for Q_{EC}. If the interaction energy corrections were not applied, the value deduced for Q_{EC} would have been about 20 eV larger. For nonzero values of the neutrino mass, the value of δM derived is fairly insensitive to the value of the neutrino mass assumed. For example, for $m_\nu=100$ eV the value deduced for δM increases by only 5.7 eV. This behavior is approximately quadratic for neutrino masses below 1 keV.

ACKNOWLEDGMENTS

The authors gratefully acknowledge R. Chrien and the staff at the high-flux beam reactor of Brookhaven National Laboratory for their assistance in the neutron irradiation. We also thank R. Lougheed, D. Sisson, and F. Bazan (Lawrence Livermore National Laboratory) for their help in the source preparation and characterization. This work was performed under the auspices of the U. S. Department of Energy by the Lawrence Livermore Laboratory under Contract No. W-7405-ENG-48.

[1]R. Barbieri, J. Ellis, and M. K. Gaillard, Phys. Lett. **90B**, 249 (1980).

[2]Edward Witten, Phys. Lett. **91B**, 81 (1980).

[3]W. C. Haxton and G. J. Stephenson, Jr. in *Progress in Particle and Nuclear Physics,* edited by D. Wilkinson (Pergamon, Oxford, 1984), p. 409.

[4]B. Pontecorvo, Zh. Eksp. Teor. Fiz. **53**, 1717 (1967) [Sov. Phys. —JETP **26**, 984 (1968)].

[5]F. Reines, Nucl. Phys. **A396**, 469c (1983).

[6]R. Davis, Jr., J. C. Evans, and B. T. Cleveland, in *Long-Distance Neutrino Detection—1978 (C.L. Cowan Memorial Symposium),* AIP Conf. Proc. No. 52, edited by A. W. Saenz and H. Uberall (AIP, New York, 1979).

[7]J. N. Bahcall, S. H. Lubow, W. F. Huebner, N. H. Magee, Jr., A. L. Merts, M. F. Argo, P. D. Parker, B. Rozanyai, and R. K. Ulrich, Phys. Rev. Lett. **45**, 945 (1980).

[8]M. S. Turner, in *Weak Interactions as Probes of Unification, (Virginia Polytechnic Institute—1980),* edited by G. B. Collins, L. N. Chang, and J. R. Ficenec, AIP Conf. Proc. No. 72, Particles and Fields Subseries No. 23 (AIP, New York, 1981).

[9]S. M. Faber and J. S. Galagher, Annu. Rev. Astron. Astrophys. **17** (1979).

[10]J. P. Ostriker and P. J. E. Peebles, Astrophys. J. **186**, 467 (1973).

[11]R. Cowsik and J. McClelland, Phys. Rev. Lett. **29**, 669 (1972).

[12]D. N. Schramm and G. Steigman, Astron. J. **243**, 1 (1981).

[13]V. S. Kozik, V. A. Lyubimov, E. G. Novikov, V. Z. Nozik, and E. F. Tret'yakov, Yad. Fiz. **32**, 301 (1980) [Sov. J. Nucl. Phys. **32**, 154 (1980)].

[14]C. L. Bennett, A. L. Hallin, R. A. Naumann, and P. T. Springer (unpublished).

[15]C. L. Bennett, A. L. Hallin, R. A. Naumann, P. T. Springer, M. S. Witherell, R. E. Chrien, P. A. Baisden, and D. H. Sisson, Phys. Lett. **107B**, 19 (1981).

[16]A. De Rujula, Nucl. Phys. **B188**, 414 (1981).

[17]P. A. Baisden, D. H. Sisson, S. Niemeyer, B. Hudson, C. L. Bennett, and R. A. Naumann, Phys. Rev. C **28**, 337 (1983).

[18]P. T. Springer, C. L. Bennett, and P. A. Baisden, Phys. Rev. A **31**, 1965 (1985).

[19]R. J. Glauber and P. C. Martin, Phys. Rev. **104**, 158 (1956).

[20]W. Gordon, Ann. Phys. (Leipzig) **2**, 1031 (1929).

[21]H. A. Bethe and E. E. Salpeter, *Quantum Mechanics of One- and Two-Electron Atoms* (Springer-Verlag, Berlin, 1957).

[22]D. Chattarji, *The Theory of Auger Transitions* (Academic, London, 1976).

[23]G. W. Pratt, Jr., Phys. Rev. **88**, 1217 (1952).

[24]K. Riisager, A. De Rujula, P. G. Hansen, B. Jonson, and H. L. Ravn, Phys. Scr. **31**, 321 (1985).

[25]James Dwight Dana, *Manual of Mineralogy,* 17th ed. (Wiley, New York, 1959), p. 236.

[26]J. C. Russ, in *Advances in X-ray Analysis,* edited by R. W. Gould, C. S. Barrett, J. B. Newkirk, and C. O. Ruud (Plenum, New York, 1976), Vol. 19, p. 161.

[27]*Handbook of Mathematical Functions,* edited by M. Abramowitz and I. A. Stegun (Dover, New York, 1972).

[28]F. X. Hartmann and R. A. Naumann, Phys. Rev. C **31**, 1594 (1985).

[29]H. L. Ravn, J. U. Andersen, G. J. Beyer, A. De Rujula, P. G. Hansen, B. Jonson, and L. Laegsgaard, in Proceedings of the XVIIIth Rencontre de Moriond, 1984 (unpublished).

[30]J. C. Slater, *Quantum Theory of Atomic Structure* (McGraw-Hill, New York, 1960), Vol. 1.

[31]J. A. Bearden and A. F. Burr, Rev. Mod. Phys. **39**, 125 (1967).

[32]K. N. Huang, M. Aoyagi, M. H. Chen, B. Crasemann, and H. Mark, At. Data Nucl. Data Tables **18**, 243 (1976).

[33]F. Herman and S. Skillman, *Atomic Structure Calculations* (Prentice-Hall, Englewood Cliffs, N.J., 1963).

[34]W. Bambynek, H. Behrens, M. H. Chen, B. Crasemann, M. L. Fitzpatrick, K. W. D. Ledingham, H. Genz, M. Mutterer, and R. L. Intemann, Rev. Mod. Phys. C **28**, 337 (1983).